solar

MDPI

Article

Experimental Comparison of Vertically Oriented Passive Thermosiphon and Integrated Solar Water Heaters Under Arid Climatic Conditions

Walid Zaafouri [1], Romdhane Ben Slama [2], Béchir Chaouachi [2], Saif Ali Kadhim [3], Abdallah Bouabidi [1,4] and Arman Ameen [5,*]

[1] Laboratory of Mechanical Modeling, Energy & Materials (LM2EM), LR24ES23, National School of Engineers of Gabes (ENIG), University of Gabes, Avenue of Omar Ib-Elkhattab, Zrig, Gabes 6023, Tunisia; walidzaafouri9@gmail.com (W.Z.); abdallah.bouabidi@issig.u-gabes.tn (A.B.)
[2] Research Laboratory: Energy, Water, Environment and Processes, National School of Engineers of Gabes (ENIG), University of Gabes, Gabes 6026, Tunisia; romdhaneb.slama@gmail.com (R.B.S.); bechir.chaouachi@enig.rnu.tn (B.C.)
[3] College of Mechanical Engineering, University of Technology-Iraq, Baghdad 10066, Iraq; 20292@uotechnology.edu.iq
[4] Higher Institute of Industrial Systems of Gabes, University of Gabes, Gabes 6072, Tunisia
[5] Department of Building Engineering, Energy Systems and Sustainability Science, University of Gävle, 801 76 Gävle, Sweden
* Correspondence: arman.ameen@hig.se

Abstract

This study experimentally compares the thermal performance of two vertically oriented passive solar water heating systems under arid outdoor conditions in Gabes, Tunisia: a thermosiphon solar water heater (TSWH) and an integrated solar water heater (ISWH). Both prototypes were installed side by side, facing south, with identical collector areas and the same climatic exposure. Experiments were conducted over two consecutive clear-sky days under no-load and load conditions. The systems were evaluated in terms of water-temperature evolution, thermal stratification, thermal efficiency, heat-retention behaviour, overall heat-loss coefficient, and useful hot-water production. The results showed that the ISWH achieved higher peak water temperatures, reaching 59.8 °C and 57.5 °C during the two test days, compared with 48.55 °C and 53.65 °C for the TSWH. The ISWH also showed higher peak thermal efficiencies of approximately 49% and 48%, while the TSWH reached approximately 41% and 40%. Under hot-water extraction conditions, the ISWH delivered about 25 L of usable hot water at 45 °C, compared with 19 L for the TSWH. However, the TSWH exhibited better thermal retention, with a lower overall heat-loss coefficient of 1.763 W/m^{2}K compared with 2.38 W/m^{2}K for the ISWH. These findings demonstrate a clear trade-off between rapid daytime heat capture and non-solar heat preservation. The ISWH is more suitable for applications requiring higher daytime hot-water production, whereas the TSWH is preferable when improved heat retention after solar input decreases is required.

Keywords: passive solar water heater; thermosiphon; integrated collector storage; thermal efficiency; heat retention; hot-water production; arid climate

Academic Editor: Andreu Moià-Pol

Received: 12 June 2026
Revised: 4 July 2026
Accepted: 9 July 2026
Published: 13 July 2026

1. Introduction

The growing demand for sustainable and energy-efficient technologies has intensified interest in renewable energy systems for domestic and building applications. Among the available renewable resources, solar energy is one of the most abundant and widely accessible sources, particularly in regions characterized by high solar irradiation [1,2]. Its direct conversion into thermal energy has attracted considerable attention because of its simplicity, low environmental impact, and suitability for a wide range of heating applications [3–7].

Within this context, solar water heating systems represent one of the most mature and practical solar thermal technologies for domestic hot-water production [8–11]. Solar water heaters are generally classified into active and passive systems [12]. Active systems employ auxi675liary mechanical devices, such as pumps and controllers, to circulate the heat-transfer fluid and regulate operation. This can provide greater controllability and potentially higher performance, but it is often associated with higher installation costs, greater maintenance requirements, and increased system complexity [13]. In contrast, passive systems operate through natural circulation and do not require mechanical pumping, making them attractive for residential applications because of their lower cost, simpler design, and improved reliability [14].

Among passive solar water heating technologies, thermosiphon solar water heaters (TSWHs) and integrated solar water heaters (ISWHs) are two widely investigated and practically adopted configurations [15,16]. Thermosiphon systems are based on the density difference between hot and cold water, which drives natural circulation between the collector and the storage tank [17,18]. These systems are well known for their robust operation and their ability to provide hot water without external energy input. Integrated solar water heaters, also known as collector-storage systems, combine the absorber and storage functions within a single unit, resulting in a compact design that can reduce installation complexity and facilitate architectural integration [16,19]. Previous studies have shown that ISWH systems can achieve high outlet or storage water temperatures under favourable climatic conditions, while thermosiphon systems are often associated with better thermal stability and heat preservation due to the physical separation between the collector and the storage tank [20,21].

A considerable body of research has examined the thermal performance, modelling, and optimization of solar water heating systems. Dynamic testing and simulation-based studies have demonstrated the importance of system-level evaluation for predicting long-term behaviour and estimating the solar contribution to domestic hot-water demand [22,23]. Other investigations have emphasized the sensitivity of system performance to climatic parameters, operating conditions, and thermal losses [18,24]. Recent developments have also explored design enhancement strategies, material improvements, and advanced heat-transfer media, including nanofluids and modified collector-storage arrangements, to improve thermal performance and energy efficiency [19,25]. In parallel, increasing attention has been given to building-integrated solar thermal technologies, especially façade-mounted and wall-integrated solutions that can improve the functional and architectural integration of solar systems in urban environments [14,26].

Despite these advances, several research gaps remain. First, many previous studies have investigated TSWH and ISWH systems separately or under different climatic and operating conditions, making direct comparison difficult [15,16,19–21,27]. Second, limited experimental attention has been given to vertically oriented passive solar water heaters, even though such configurations are particularly relevant for façade integration in buildings and for applications where roof space is limited [28]. Third, while daytime thermal efficiency is frequently reported, the trade-off between heat capture during solar exposure and thermal retention during non-solar periods has received less systematic experimental analysis under comparable outdoor conditions. This trade-off is especially important in arid regions, where high daytime solar availability can enhance heat gain, but thermal losses may significantly influence hot-water availability outside peak sunshine hours.

Therefore, the aim of this study is to experimentally compare the thermal performance of two vertically oriented passive solar water heating systems, namely a thermosiphon solar water heater and an integrated solar water heater, under the same outdoor climatic conditions in Gabes, Tunisia. The comparison focuses on temperature evolution, thermal efficiency, thermal retention, and useful hot-water production under both no-load and load conditions.

The novelty of this work lies in the direct side-by-side experimental evaluation of two passive solar water heater configurations installed with the same vertical orientation, similar collector dimensions, and identical climatic exposure. Unlike studies in which TSWH and ISWH systems are evaluated separately, the present experimental framework enables a more consistent comparison of their thermal behaviour, hot-water production, and heat-retention characteristics. In addition, the study explicitly highlights the trade-off between daytime heat capture and non-solar heat retention, which is important for selecting suitable passive solar water heater configurations according to user demand patterns and operating conditions.

The findings of this study provide useful guidance for engineers, designers, and decision-makers involved in selecting solar thermal systems for arid and high-solar-radiation regions. In particular, the results help distinguish between configurations that favour rapid daytime heat gain and those that ensure better thermal retention after solar input decreases. Such information is valuable for improving the design and deployment of passive solar water heaters in residential buildings and building-integrated solar thermal applications.

2. Materials and Methods

2.1. Materials

Two passive solar water heating systems were investigated in this study: an integrated solar water heater (ISWH) and a thermosiphon solar water heater (TSWH). The two systems were designed with the same external dimensions of 2.0 m × 1.0 m × 0.225 m, allowing their thermal performance to be compared under similar geometric and climatic boundary conditions. Although both systems use comparable basic components, they differ in their structural configuration, absorber design, and heat-storage arrangement. A summary of the main components and materials is presented in Table 1, while the system configurations are illustrated in Figures 1 and 2.

Table 1. Comparison of the main components of the ISWH and TSWH prototypes.

Component	ISWH	TSWH
Heat exchanger	Serpentine copper tube; 20 coils; outer diameter = 0.014 m; inner diameter = 0.012 m	Serpentine copper tube; 20 coils; outer diameter = 0.014 m; inner diameter = 0.012 m
Insulation	Polystyrene and glass wool	Polystyrene and glass wool
Frame/support structure	Wooden casing with brick masonry support	Redwood frame
Absorber	Black-painted concrete surface	Black-painted galvanized steel sheet; thickness = 0.001 m; length = 2 m; width = 1 m
Transparent cover	Glass cover; thickness = 0.006 m	Glass cover; thickness = 0.006 m

https://doi.org/10.3390/solar6040041

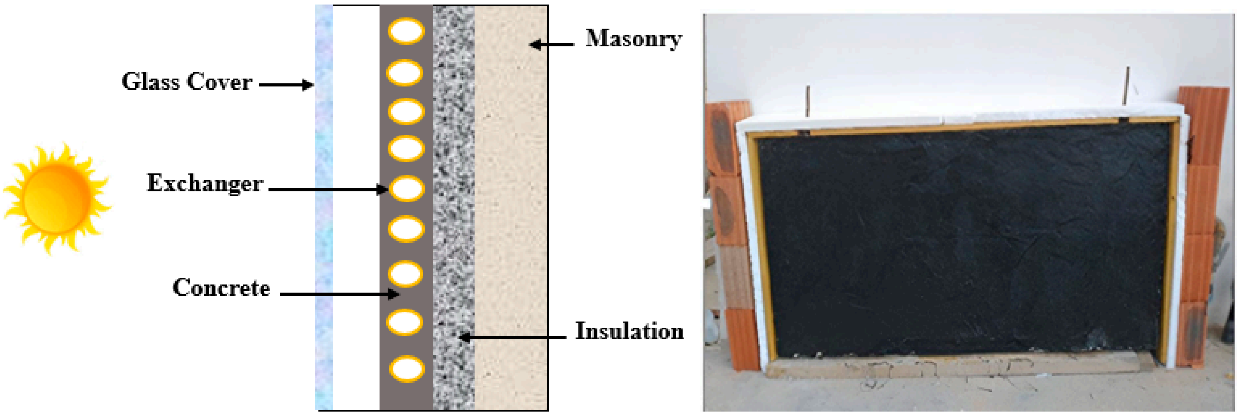

Figure 1. Integrated solar water heater (ISWH).

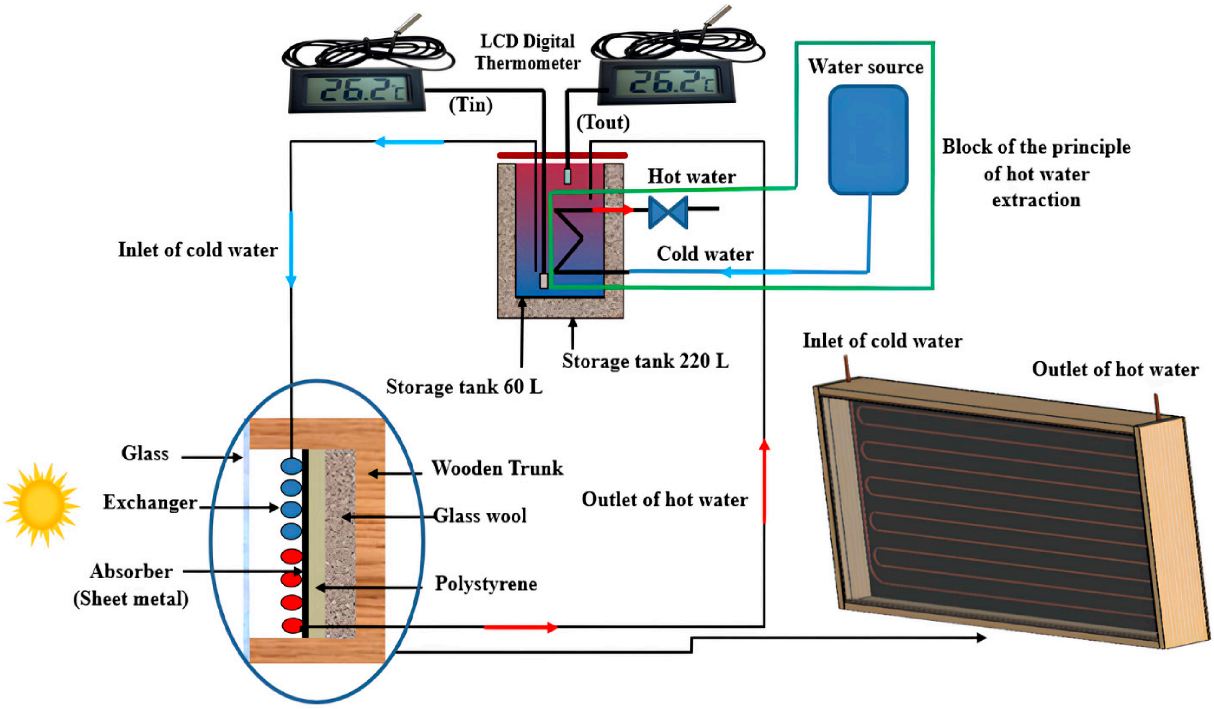

Figure 2. Thermosiphon solar water heater (TSWH).

Both systems use a serpentine copper heat exchanger consisting of 20 coils, with an outer diameter of 14 mm and an inner diameter of 12 mm. Copper was selected because of its high thermal conductivity, corrosion resistance, and suitability for solar thermal applications. However, the integration of the heat exchanger differs between the two designs.

In the ISWH configuration, shown in Figure 1, the serpentine copper tube is embedded within a black-painted concrete slab, which acts as both the solar absorber and the thermal storage medium. The slab is enclosed in a wooden casing and insulated with a 50 mm thick polystyrene layer, while brick masonry provides structural support and additional thermal mass. The exposed absorber surface is coated with black paint to improve solar radiation absorption. A 6 mm thick glass cover is used as the transparent glazing to allow solar radiation transmission while reducing convective heat losses. This compact collector-storage configuration enables direct heat transfer and is suitable for building-integrated applications.

In contrast, the TSWH system, shown in Figure 2, follows a separated collector-storage configuration. The absorber consists of a galvanized steel plate with dimensions of 2.0 m × 1.0 m × 1 mm, coated with matte black paint to enhance solar absorption. The dimensional details of the absorber plate are shown in Figure 3. The absorber is mounted within a redwood frame and insulated on the back and sides using polystyrene and glass wool to reduce heat losses. The serpentine copper heat exchanger is attached to the rear side of the absorber plate to increase the heat-transfer area. A 6 mm thick glass cover is also used as the transparent glazing to allow solar radiation transmission while reducing convective heat losses. Unlike the ISWH, the TSWH relies on natural circulation driven by the thermosiphon effect, in which heated water rises from the collector to the storage tank without mechanical assistance.

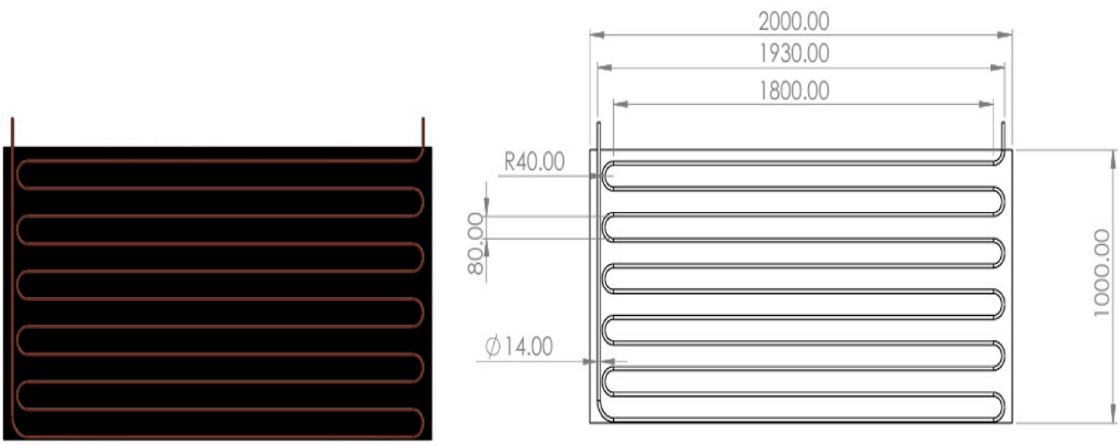

Figure 3. Dimensional details of the galvanized steel absorber plate used in the TSWH prototype.

Overall, the ISWH integrates heat absorption and storage within a single compact unit, whereas the TSWH separates the collector and storage tank and depends on buoyancy-driven circulation. These different configurations are expected to influence heat gain, thermal losses, heat retention, and hot-water availability.

The materials and geometrical configurations were selected based on practical considerations, including local availability, cost-effectiveness, ease of manufacturing, and suitability for building integration. Materials such as brick, concrete, wood, galvanized steel, copper tubing, polystyrene, glass wool, and glass are readily available in the Tunisian market and are commonly used in solar thermal applications. The systems were designed for operation in arid regions with high solar irradiation, such as southern Tunisia. Therefore, the main objective was to evaluate the thermal performance and practical feasibility of the two configurations under real outdoor climatic conditions, rather than to conduct a detailed geometrical optimization.

The thermophysical properties of the main materials used in the solar water heater prototypes are listed in Table 2.

Table 2. Thermophysical properties of the main materials used in the solar water heater prototypes.

Property	**Absorber**		**Transparent Cover**	**Insulation**
Material	Steel sheet	Concrete	Glass	Wood Polystyrene
Specific heat (J/kgK)	502.48	880	840	2310 1423
Thermal conductivity k (W/mK)	16	1.4	1.1	0.173 0.034
Density ρ (kg/m^3)	8030	2300	2700	700 19.8

2.2. Experimental Methodology

The experimental study was conducted in Gabes, Tunisia (33°50′57″ N, 10°6′14″ E), on 13 and 14 March 2023 under real outdoor climatic conditions. The objective was to evaluate and compare the thermal performance of the thermosiphon solar water heater (TSWH) and the integrated solar water heater (ISWH). Both systems were installed side by side, vertically oriented, and facing due south in order to maximize solar exposure and simulate façade-integrated operation (see Figure 4). Each unit had a collector area of 2.0 m^2, ensuring identical geometric and environmental boundary conditions for a consistent comparison.

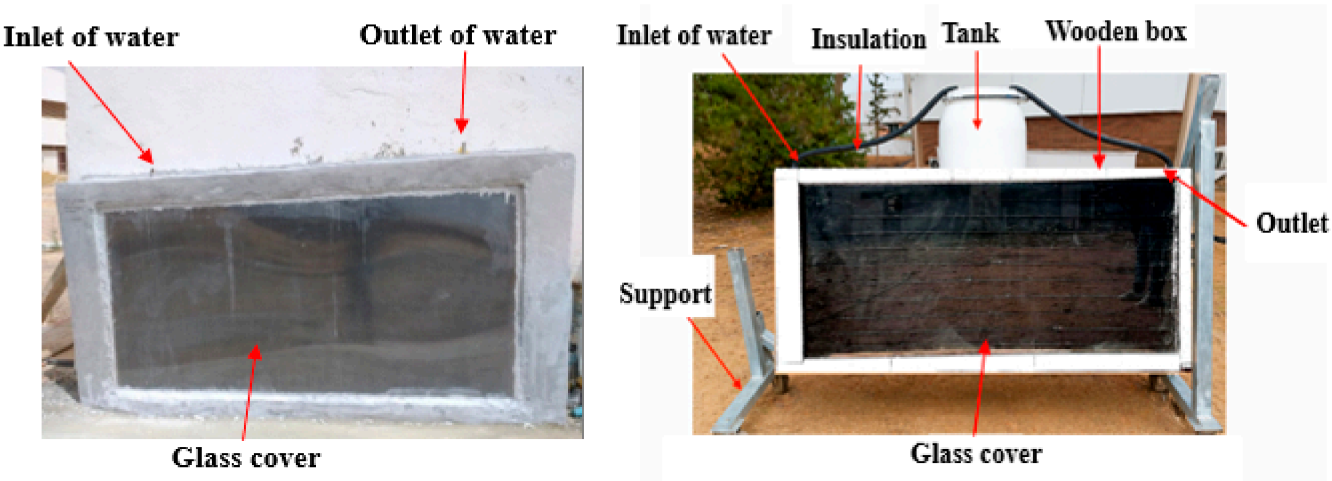

Figure 4. Photograph of the vertically oriented ISWH and TSWH prototypes during outdoor testing.

Two experimental scenarios were investigated. On the first day, 13 March 2023, the systems were operated under no-load conditions, without hot-water extraction. This test was used to analyze heat accumulation, water-temperature evolution, thermal stratification, and heat-storage behaviour. On the second day, 14 March 2023, controlled hot-water extraction was introduced to evaluate the ability of each system to provide useful hot water under load conditions. This two-day procedure enabled the comparison of both thermal performance and practical hot-water production capacity.

The experimental data were collected manually using the measurement instruments shown in Figure 5. Water temperature was measured using LCD digital thermometers with an accuracy of ±1 °C. The thermometers were installed at three vertical positions in each storage volume: bottom, middle, and top. This arrangement made it possible to monitor temperature distribution and thermal stratification inside the systems. Ambient air temperature was measured using an HTC-1 electronic thermometer with an accuracy of ±1 °C. Solar irradiance was measured using a solar power meter with an accuracy of ±10 W/m^2, positioned in alignment with the transparent cover of the solar water heater.

All measurements were recorded hourly between 08:00 and 19:00 under the same outdoor environmental conditions. During the second experimental day, hot water was extracted whenever the outlet temperature exceeded 45 °C, which was adopted as the minimum useful temperature for domestic hot-water use. The extracted water volume was measured over time and used to compare the hot-water production capacity of the two systems.

https://doi.org/10.3390/solar6040041

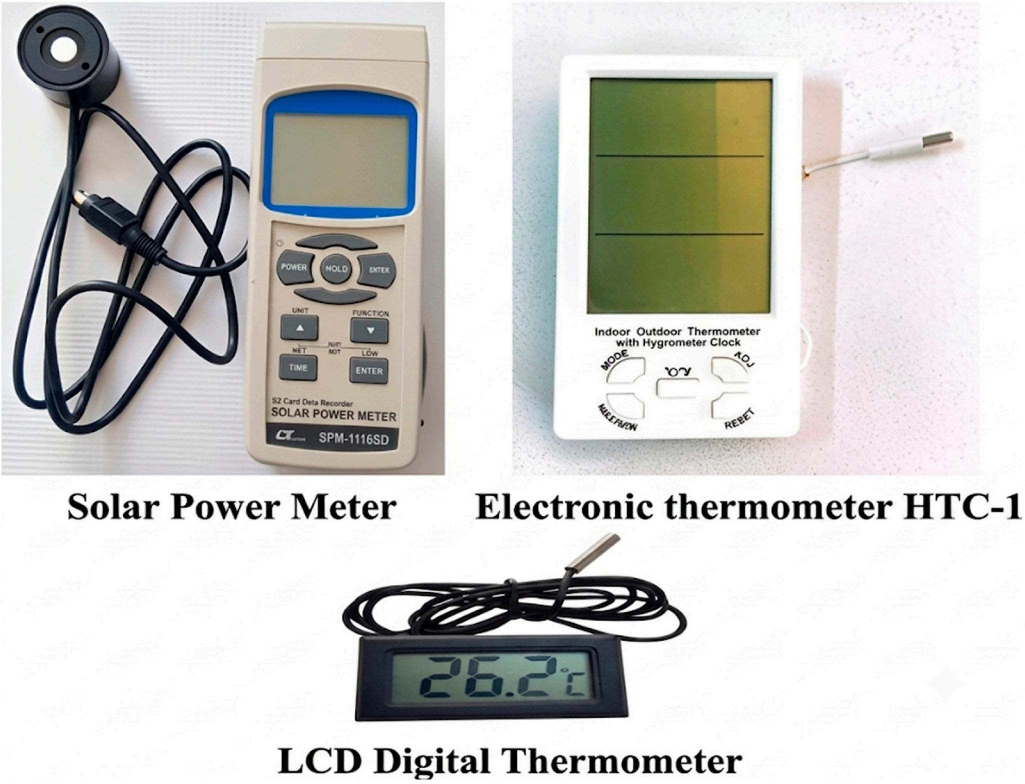

Figure 5. Measurement instruments used during the experimental tests.

3. Energy Analysis

Thermal performance is a key parameter for evaluating and comparing the two manufactured solar water heater prototypes. In this study, the performance of the systems was assessed using the input–output method, also referred to as the black-box method [29]. In this approach, the incident solar energy received by the collector surface is considered as the energy input, while the useful thermal energy gained by the water is considered as the energy output. During the experiments, the systems were exposed to solar radiation under real outdoor conditions, and the water temperature, ambient temperature, and incident solar irradiance were measured at hourly intervals.

$$\eta = \frac{mC_p\Delta T}{SG\Delta t} \tag{1}$$

where

m is the mass of water (kg).

C_p is the specific heat capacity of water (J/kgK).

ΔT represents the hourly increase in the average water temperature, calculated as the difference between 2 consecutive hourly measurements ($T_{i+1} - T_i$) (°C).

S is the collector surface area (m^2).

G is the measured solar irradiance incident on the collector surface (W/m^2), and Δt is the measurement time interval (s).

Since the experiments were under real outdoor conditions, both solar irradiance and ambient temperature varied continuously throughout the day, resulting in transient operating conditions. Therefore, the thermal efficiency was calculated at each hourly interval using the measured hourly solar irradiance and the corresponding hourly increase in the average water temperature.

To estimate the overall heat-loss coefficient, the systems were heated throughout the day under solar radiation until the water temperature reached its maximum value. The water temperature inside the tank was measured at three vertical positions (bottom, middle, and top), and the ambient temperature was recorded at 17:00. After sunset, the systems were allowed to cool naturally overnight, and both the water temperature and ambient temperature were measured again at 08:00 the following morning [30].

The heat-loss coefficient was then determined using the following expression:

$$U_L = \frac{\rho C_p V}{S \Delta t} ln \frac{(T_i - T_{am})}{\left(T_f - T_{am}\right)} \tag{2}$$

where

U_L is the thermal loss coefficient (W/m^{2}K).
ρ is the density of water (kg/m^3).
C_p is the specific heat capacity of water (J/kgK).
V is the volume of water in the tank (m^3).
S is the collector surface area (m^2).
Δt is the cooling time interval (s).
T_i is the initial water temperature (°C).
T_f is the final water temperature (°C).
T_{am} is the ambient temperature during the cooling period (°C).

4. Results and Discussion

Experiments were conducted on 13 and 14 March 2023 under clear-sky outdoor conditions in Gabes, Tunisia. The first test day was carried out under no-load conditions, while the second test day included hot-water extraction. The analysis focused on the temporal variation in solar radiation, ambient temperature, water temperature, thermal efficiency, heat-retention behaviour, and useful hot-water production.

4.1. Without Hot-Water Extraction

Figure 6 shows the hourly variation in solar flux and ambient temperature on 13 March 2023. The solar flux increased gradually during the morning, reached a maximum value of approximately 712 W/m^2 around midday, and then decreased progressively during the afternoon. The ambient temperature followed a similar daily trend, increasing during the first part of the day and declining later as solar input decreased. This behaviour reflects the typical daytime variation in outdoor climatic conditions under clear-sky operation.

The trends shown in Figure 6 provide the environmental basis for interpreting the thermal response of both solar water heater prototypes. Since the TSWH and ISWH were tested simultaneously under the same outdoor conditions, the measured differences in water temperature and thermal efficiency can mainly be attributed to differences in system configuration, heat-transfer mechanism, and heat-storage behaviour rather than to differences in climatic exposure.

Figure 7 presents the variation in water temperature at three vertical levels in the TSWH tank on 13 March 2023. The water temperature increased at all measured levels during the day as solar radiation increased. A clear thermal stratification pattern was observed, with the highest temperature recorded at the top of the tank, followed by the middle and bottom levels. This behaviour is expected in thermosiphon systems because heated water rises due to buoyancy, while colder water remains near the bottom of the tank. The maximum temperature at the top of the TSWH tank reached approximately 56.2 °C at 16:00. This indicates that the system was able to collect and store solar energy effectively under the tested outdoor conditions. The observed stratification is beneficial for domestic hot-water use because it allows hotter water to be available near the upper outlet region, even when the lower part of the tank remains at a lower temperature.

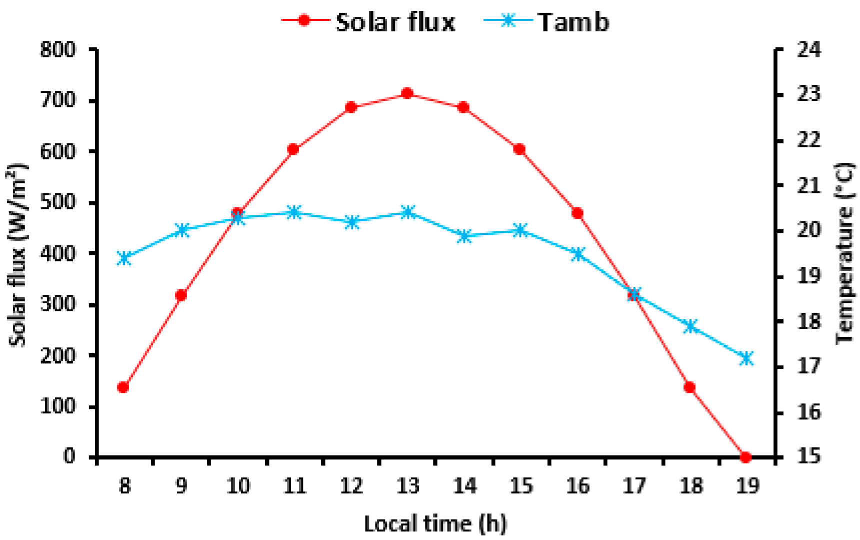

Figure 6. Hourly variation in solar flux and ambient temperature on 13 March 2023.

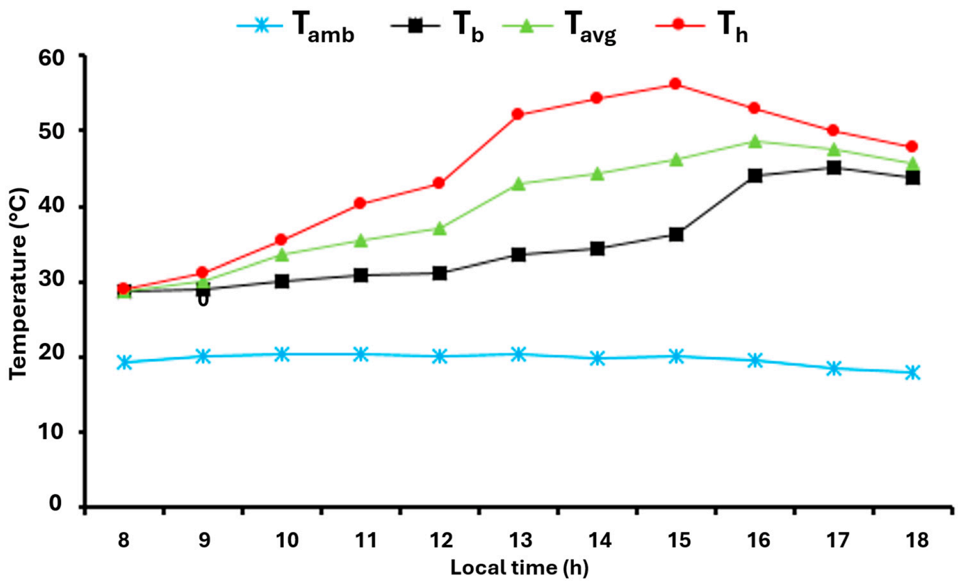

Figure 7. Hourly variation in ambient temperature and water temperature at three vertical levels in the TSWH tank on 13 March 2023.

Figure 8 illustrates the evolution of solar flux, ambient temperature, and average water temperature for both systems on 13 March 2023. Solar radiation gradually increases from 137 W/m^2 at 9:00 h to a peak value of 712 W/m^2 around 13:00 h, before progressively decreasing during the late afternoon. The ambient temperature exhibits a similar trend, rising from 19.4 °C in the early morning to approximately 20.4 °C during daylight hours, then decreasing slightly in the afternoon. The maximum water temperature reaches 59.8 °C for the ISWH (Figure 8b) at approximately 15:00 h. In contrast, the TSWH exhibited comparatively lower peak temperatures, reaching a maximum water temperature of 48.55 °C around 15:00 h, as shown in Figure 8a, because of the physical separation between the collector and the storage tank, as well as its dependence on buoyancy-driven natural circulation, which introduces additional thermal inertia and heat-transfer limitations.

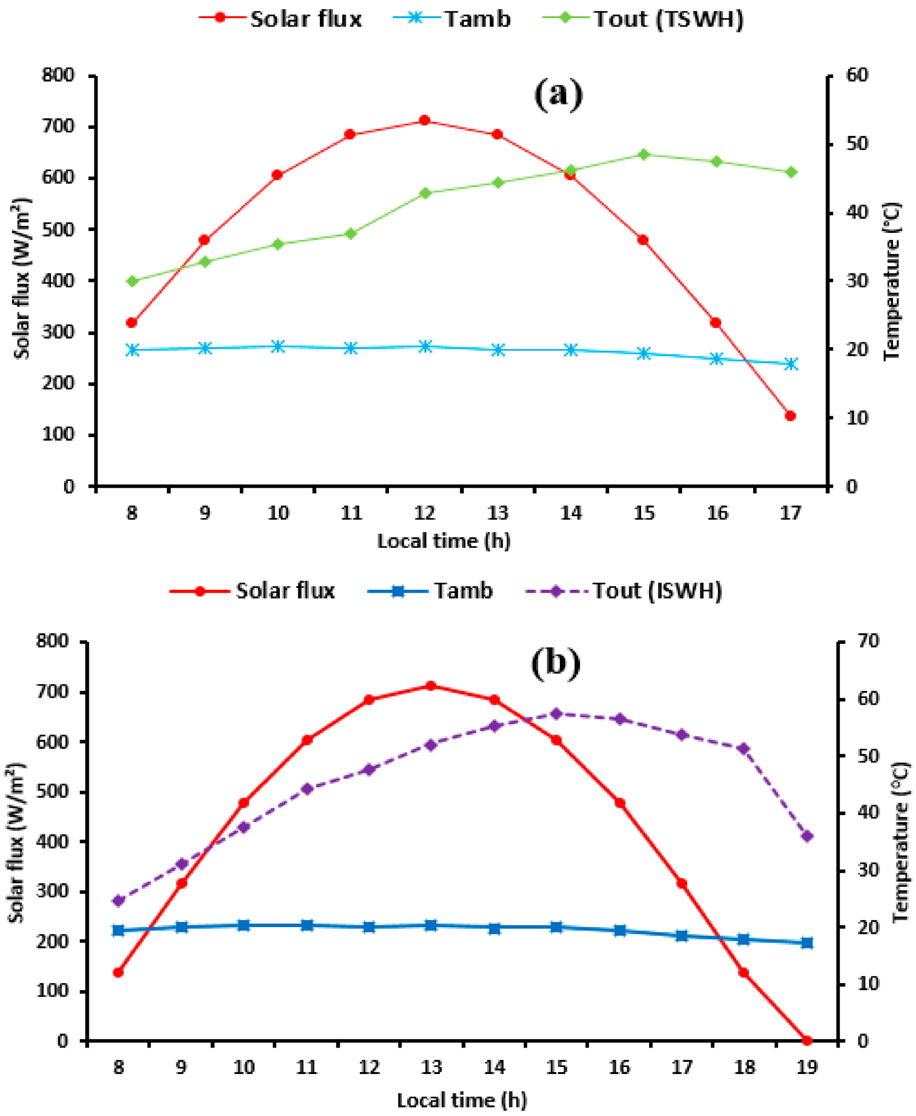

Figure 8. Hourly variation in solar flux, ambient temperature, and average water temperature on 13 March 2023: (**a**) TSWH and (**b**) ISWH.

After 15:00 h, as the solar flux gradually decreases, the water temperature in the TSWH declines slowly, reaching 43.2 °C at 19:00 h, whereas it decreases more rapidly in the ISWH, attaining 37 °C at the same time.

Figure 9 shows the relationship between thermal efficiency and normalized gain, $\Delta T/G$, for the two systems on 13 March 2023. Figure 9a presents the results for the TSWH, while Figure 9b presents the corresponding results for the ISWH. The normalized gain represents the ratio between the temperature difference and the incident solar irradiance, and it is commonly used to evaluate the thermal behaviour of solar collectors.

For the TSWH, the thermal efficiency decreased from approximately 27.5% at a normalized gain of 0.0255 m^2K/W to about 19% at 0.049 m^2K/W. For the ISWH, the efficiency decreased from approximately 49% at a normalized gain of 0.038 m^2K/W to about 8% at 0.065 m^2K/W. This decreasing trend is consistent with solar collector behaviour, where higher values of $\Delta T/G$ indicate a larger temperature difference between the system and the surrounding environment relative to the available solar input. As this difference increases, convective and radiative heat losses become more significant, leading to a reduction in thermal efficiency.

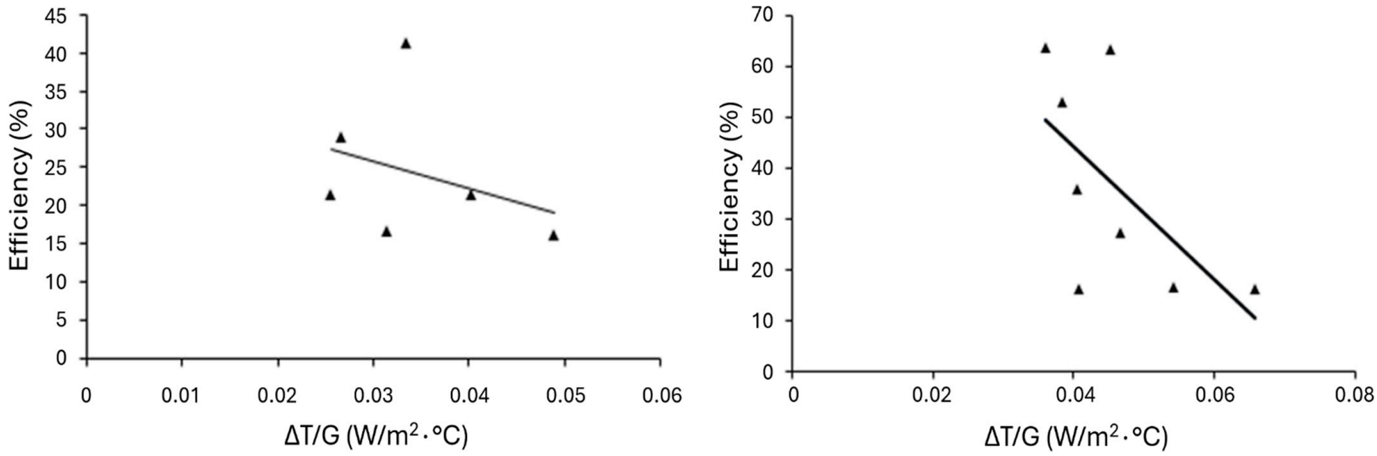

(**a**) (**b**)

Figure 9. Thermal efficiency as a function of normalized gain on 13 March 2023: (**a**) TSWH and (**b**) ISWH.

The scatter observed in the experimental data can be attributed to transient outdoor conditions, including fluctuations in solar irradiance, ambient temperature, wind effects, thermal stratification, and system thermal inertia. These factors influence the instantaneous energy balance of the systems and explain deviations from an ideal linear efficiency curve.

Figure 10 shows the hourly variation in thermal efficiency for the two systems on 13 March 2023. Figure 10a presents the TSWH efficiency, while Figure 10b presents the ISWH efficiency. Both systems showed an increase in efficiency during the morning as solar irradiance increased and the collectors absorbed more thermal energy. The efficiency then reached a peak around midday to early afternoon, when the balance between solar energy input and thermal losses was most favourable.

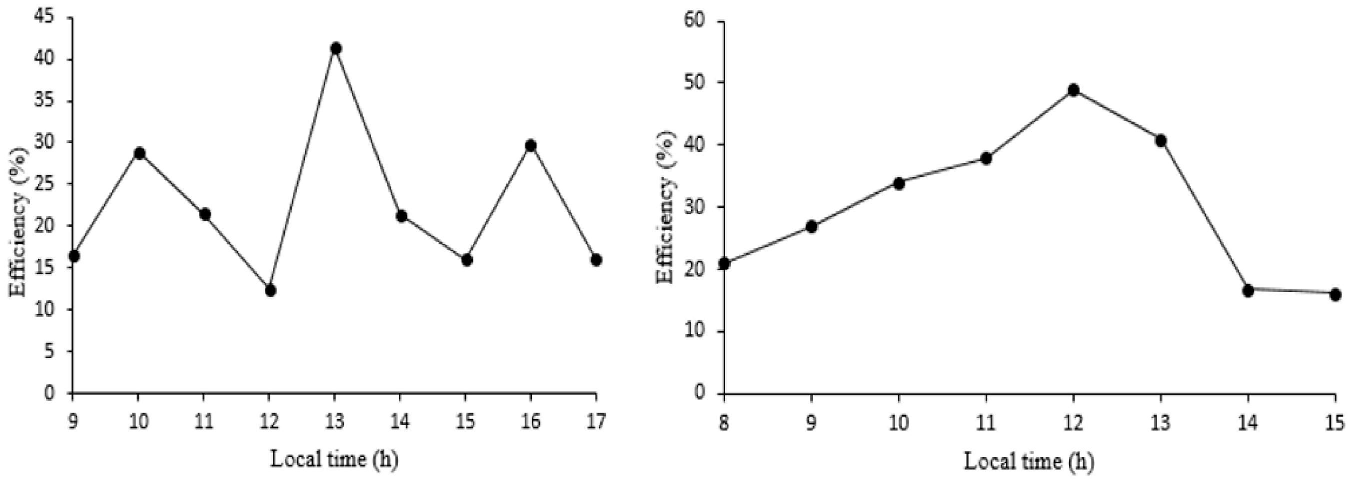

(**a**) (**b**)

Figure 10. Hourly variation in thermal efficiency on 13 March 2023: (**a**) TSWH and (**b**) ISWH.

The TSWH reached a maximum thermal efficiency of approximately 41%, whereas the ISWH reached a higher maximum efficiency of approximately 49%. The higher efficiency of the ISWH can be attributed to its integrated collector-storage configuration, which enables more direct heat transfer between the absorber and the stored water. This reduces thermal resistance during periods of strong solar radiation and allows the ISWH to respond more rapidly to increasing solar input.

After the peak period, the efficiencies of both systems decreased as solar irradiance declined and the temperature difference between the stored water and the ambient air increased. The ISWH showed a more pronounced decrease, which is consistent with its higher heat-loss tendency during the late afternoon. In contrast, the TSWH maintained a more gradual reduction in efficiency, reflecting its better thermal retention due to the separation between the collector and the insulated storage tank.

4.2. With Hot-Water Extraction

During operation, solar energy heats the water contained in the 60 L storage tank, which acts as the primary thermal storage. Domestic water does not mix with water in this tank. Instead, cold water from the water supply flows through the submerged internal heat exchanger into the 60 L tank where it absorbs heat before leaving the system as hot water.

When the water stored in the 60 L tank reaches a sufficiently high temperature, the hot-water sampling test is initiated by opening the outlet valve. The water temperature at the outlet is monitored continuously and extraction ends when it drops to 45 °C, which has been selected as the minimum acceptable temperature for domestic hot-water use. During sampling, cool cold water continuously enters the heat exchanger directly from the water supply to replace the extracted water.

After the extraction is completed, the outlet valve is closed and the system continues to operate under solar heating. The same extraction procedure is repeated every hour until the temperature of the water in the 60 L tank has decreased.

The same experimental procedure was repeated on 14 March 2023, but with controlled hot-water extraction from the two systems. Figure 11 shows the hourly variation in solar flux and ambient temperature during this test day. Solar radiation was relatively low in the early morning and then increased progressively, reaching a maximum value of approximately 708 W/m^2 around 13:00. The ambient temperature also increased during the morning, rising from approximately 15.2 °C at 08:00 to about 28.2 °C at 14:00, before decreasing later in the afternoon.

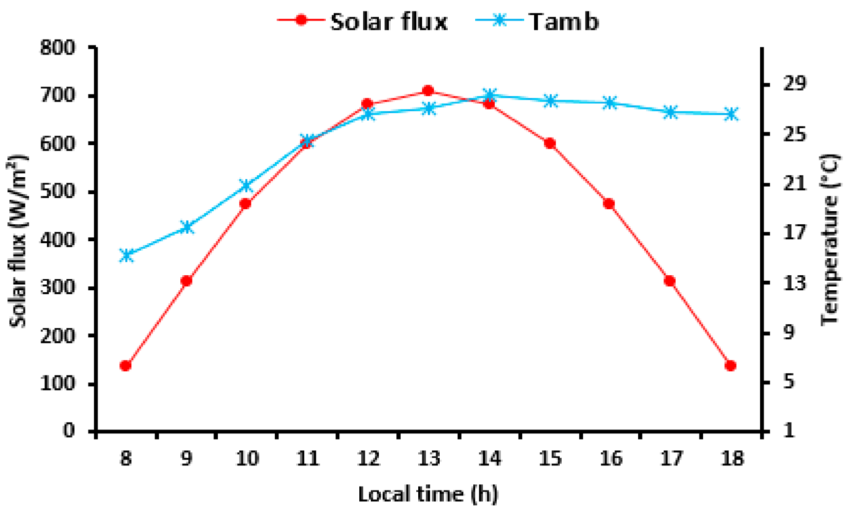

Figure 11. Hourly variation in solar flux and ambient temperature on 14 March 2023.

These climatic conditions provided a suitable basis for evaluating the thermal response of both systems under load operation. The increase in solar radiation during the morning promoted water heating, while the subsequent decrease in solar input during the afternoon influenced both the thermal efficiency and the useful hot-water production. Since both prototypes were tested simultaneously under the same outdoor conditions, the differences observed during this day mainly reflect the effect of system configuration and heat-storage behaviour under water-extraction conditions.

Figure 12 exhibits the TSWH over the course of the day on 14 March 2023, the difference in water temperature at three different levels, bottom, middle, and top, inside. These temperature profiles reflect the natural thermal stratification of the storage tank, in which colder water remains at the bottom and hotter water goes to the top. Because there is no sunlight input overnight, the water temperature in the morning begins low at all levels. The water temperature at all levels rises continuously as sun radiation rises; top level always shows the highest temperatures; middle and bottom levels follow in order. This is predicted since heated water rises due to natural convection to the tank top. At about 2:00 PM, the top highest temperature of around 57.1 °C shows how well the system captures and stores heat under sunny conditions. The water temperatures at all levels start to progressively drop in the afternoon when solar radiation starts to drop, suggesting heat loss to the ambient environment. This temperature stratification emphasizes the need for good thermal insulation to reduce heat loss and keep useable hot water for most hours of the evening. Figure 10 shows generally how effectively the TSWH gathers solar energy, heats water by free convection and creates a steady temperature gradient all day.

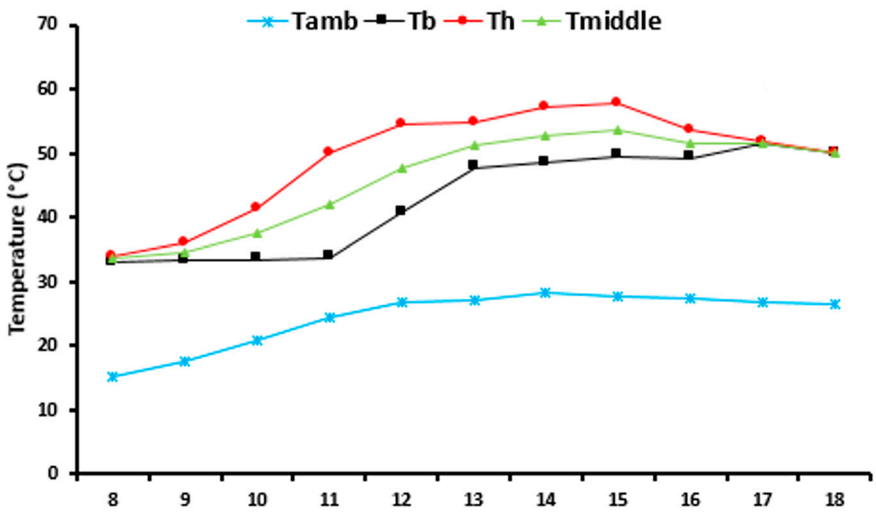

Figure 12. Hourly variation in ambient temperature and water temperature at three vertical levels in the TSWH tank on 14 March 2023.

Figure 13 presents the hourly variation in solar flux, ambient temperature, and average water temperature for the two systems on 14 March 2023. Figure 13a shows the results for the TSWH, while Figure 13b shows the corresponding results for the ISWH. The solar flux increased during the morning and reached its maximum value around 13:00, while the ambient temperature increased from approximately 15.2 °C at 08:00 to about 28.2 °C at 14:00. As shown in Figure 13a, the average water temperature in the TSWH increased gradually during the day and reached a maximum value of approximately 53.65 °C at 15:00. In comparison, Figure 13b shows that the ISWH reached a higher maximum average water temperature of approximately 57.5 °C at the same time. The higher temperature of the ISWH indicates its stronger capacity for rapid daytime heat gain under solar exposure. After the peak temperature was reached, both systems showed a decrease in water temperature as solar radiation declined and hot-water extraction continued. However, the ISWH exhibited a faster temperature decrease than the TSWH. This suggests that the ISWH performs better in terms of daytime heat capture and useful hot-water production, whereas the TSWH provides more stable thermal retention during the later part of the day.

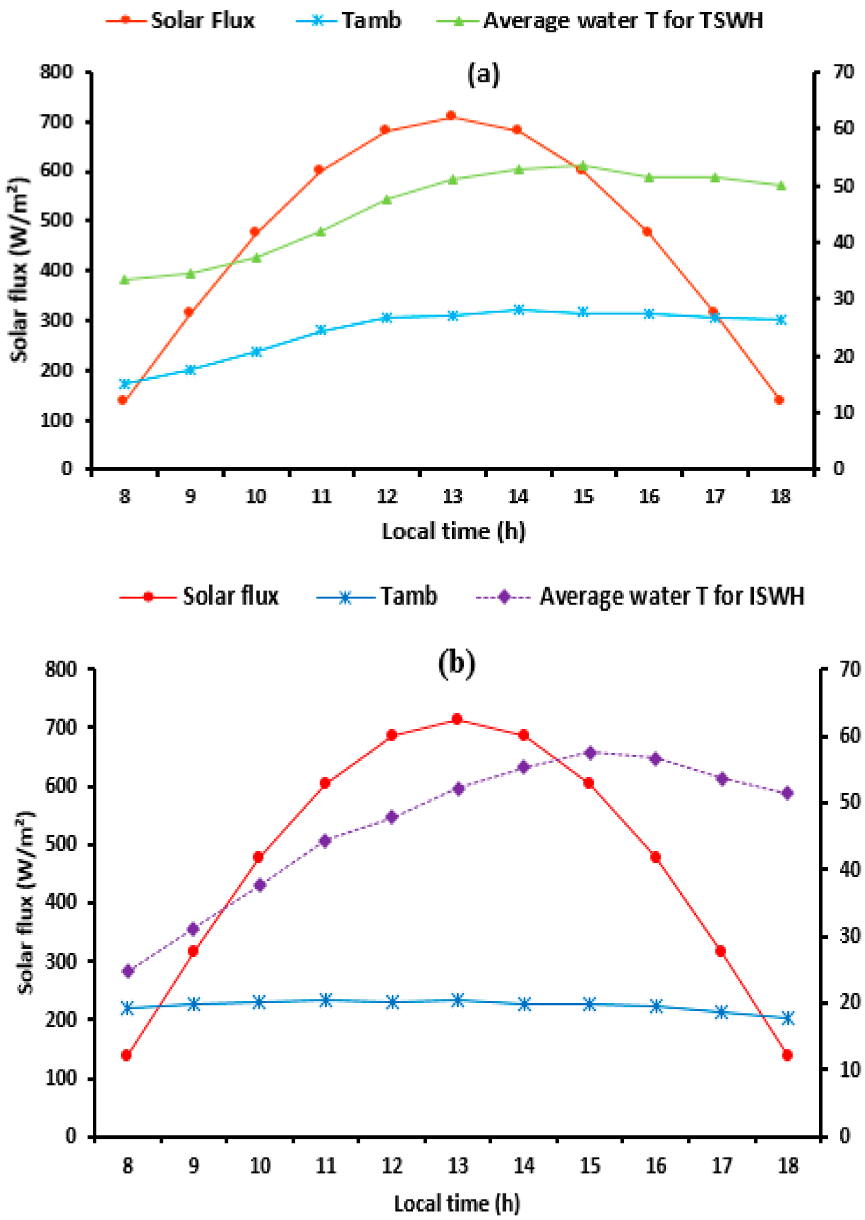

Figure 13. Hourly variation in solar flux, ambient temperature, and average water temperature on 14 March 2023: (**a**) TSWH and (**b**) ISWH.

As illustrated in Figure 14, the linear regression analysis represents the thermal efficiency behaviour of both configurations as a function of the normalized temperature gain (ΔT/G). For the TSWH system (Figure 14a), the regression yields the equation $y = -857.4x + 54.462$ with $R^2 = 0.4015$, while the ISWH system (Figure 14b) follows the equation $y = -1415.1x + 84.033$ with $R^2 = 0.4925$. The moderate R^2 values and the noticeable scatter of the experimental data points are primarily attributed to the transient and dynamic nature of outdoor testing on 14 March 2023.

For the TSWH, the thermal efficiency reached approximately 30% at a normalized gain of 0.03 m^2K/W and decreased to about 8% at a normalized gain of 0.054 m^2K/W. For the ISWH, the thermal efficiency reached approximately 32% at a normalized gain of 0.032 m^2K/W and decreased to about 18% at a normalized gain of 0.054 m^2K/W.

This decreasing trend is consistent with solar collector behaviour, as higher normalized gain values indicate increased thermal losses relative to the available solar input.

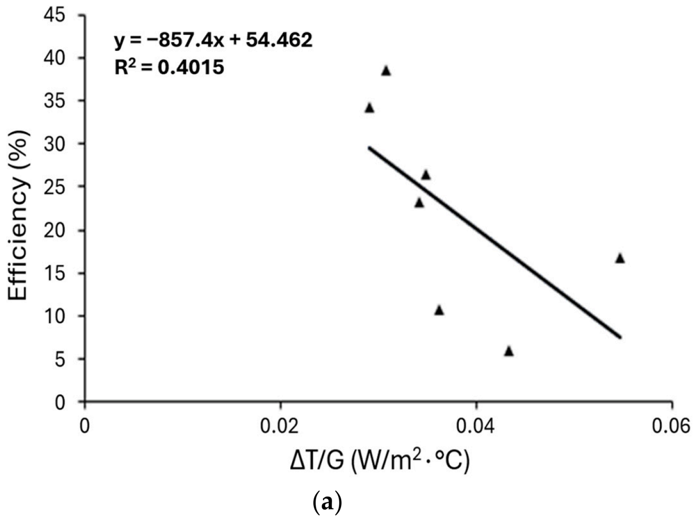

Figure 14. Thermal efficiency as a function of normalized gain on 14 March 2023: (**a**) TSWH and (**b**) ISWH.

Figure 15 presents the hourly variation in thermal efficiency for the two systems on 14 March 2023. Figure 15a shows the TSWH, while Figure 15b shows the ISWH. Both systems showed an increase in efficiency during the morning as solar irradiance increased and more thermal energy was transferred to the water. The efficiency then reached a maximum during the period of strong solar radiation, before decreasing later in the day as solar input declined and heat losses became more significant.

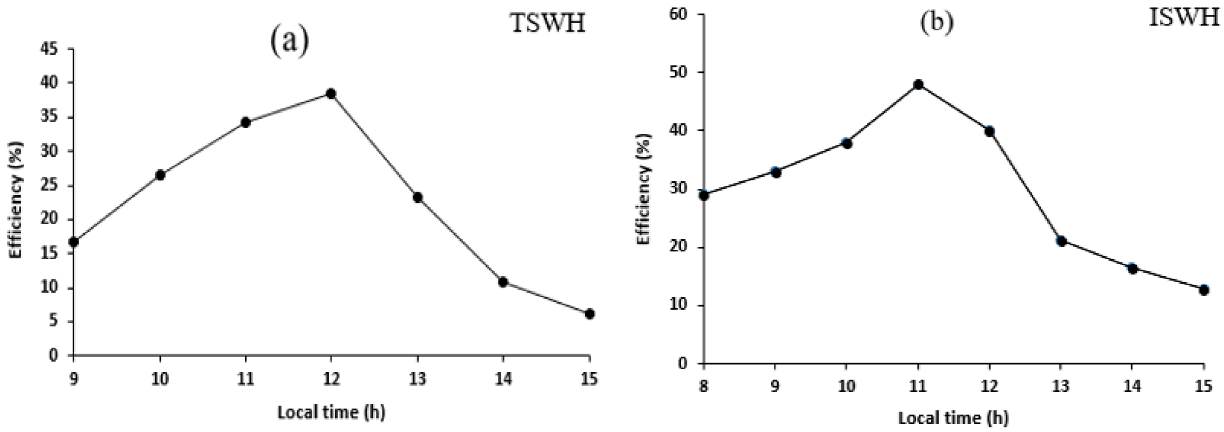

Figure 15. Hourly variation in thermal efficiency on 14 March 2023: (**a**) TSWH and (**b**) ISWH.

The TSWH reached a maximum thermal efficiency of approximately 40%, whereas the ISWH reached a higher maximum efficiency of approximately 48%. The higher efficiency of the ISWH is mainly related to its integrated collector-storage design, which promotes more direct heat transfer from the absorber to the stored water. This configuration allows the ISWH to respond more rapidly to increasing solar radiation and to achieve higher daytime thermal performance.

However, the ISWH also showed a sharper decrease in efficiency during the later part of the day. This behaviour can be attributed to its higher heat-loss tendency when the stored water temperature is elevated and solar input begins to decline. In contrast, the TSWH exhibited a more gradual reduction in efficiency, indicating better thermal stability and improved heat retention. Overall, Figure 15 confirms the trade-off observed throughout the experiments: the ISWH provides stronger daytime heat capture, while the TSWH maintains more stable thermal performance during periods of decreasing solar radiation.

To evaluate useful hot-water production, a threshold temperature of 45 °C was adopted as the minimum temperature for domestic hot-water use. During the water-extraction test on 14 March 2023, hot water was drawn from each system whenever the outlet temperature exceeded this threshold. The extracted volume was recorded as a function of local time, as shown in Figure 16.

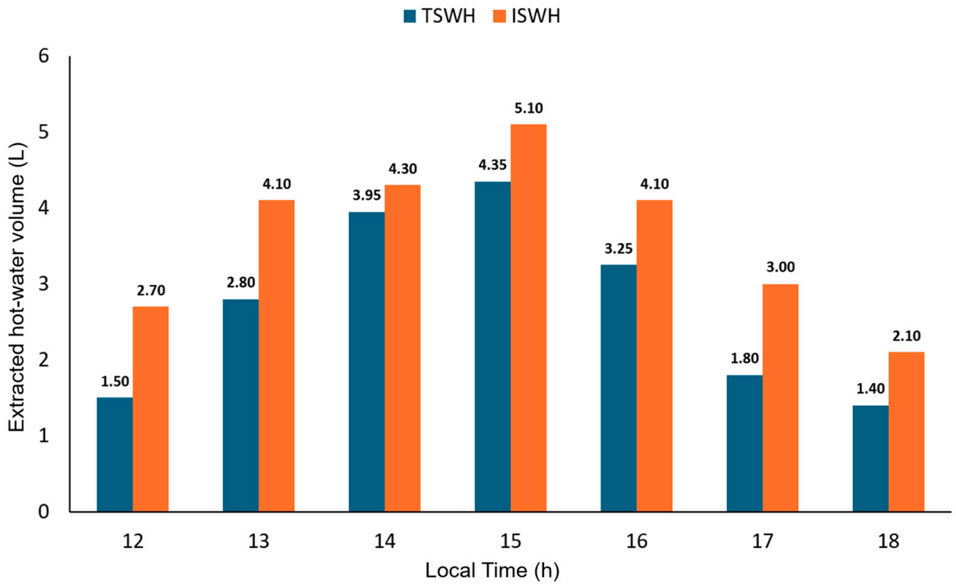

Figure 16. Hourly extracted hot-water volume from the TSWH and ISWH on 14 March 2023.

The extracted hot-water volume increased from midday and reached its maximum around 15:00, corresponding to the period when the stored water temperature was highest. After this time, the extracted volume decreased as solar radiation declined and the water temperature in the systems began to fall. The ISWH produced a larger volume of usable hot water than the TSWH throughout most of the extraction period.

The total useful hot-water production was approximately 25 L for the ISWH and 19 L for the TSWH. This difference is consistent with the higher daytime water temperatures achieved by the ISWH under load conditions. The results indicate that the integrated collector-storage configuration is more effective for rapid daytime hot-water production, whereas the TSWH offers better thermal retention after solar input decreases.

The overall heat-loss coefficient was experimentally estimated using the overnight cooling method described in Formula (2). Figure 17 shows that the overall heat-loss coefficient of the ISWH (2.38 W/m^{2}K) is significantly higher than that of the TSWH (1.763 W/m^{2}K). This difference can be attributed to the structural configuration of the two prototypes. In the TSWH, the storage tank is separated from the collector and benefits from better thermal insulation, which reduces heat exchange with the surrounding environment. In contrast, the ISWH integrates the absorber and storage unit into a single structure, resulting in a larger exposed heat-transfer surface and consequently higher conductive, convective, and radiative heat losses during non-solar periods. Although the ISWH achieves higher water temperatures during the daytime, its larger heat-loss coefficient explains the faster temperature decay observed after sunset, whereas the TSWH exhibits superior thermal retention capacity.

Table 3 compares the thermal performance obtained in the present study with selected previous experimental studies on passive solar water heaters under different climatic conditions. The comparison shows that the proposed vertically oriented systems achieved water temperatures and thermal efficiencies within, or above, the ranges reported in earlier studies. In particular, the ISWH reached a maximum water temperature of 59.8 °C and a maximum thermal efficiency of 49%, while the TSWH reached 53.65 °C and 41%, respectively. These results indicate that both configurations provide competitive thermal performance under arid outdoor conditions.

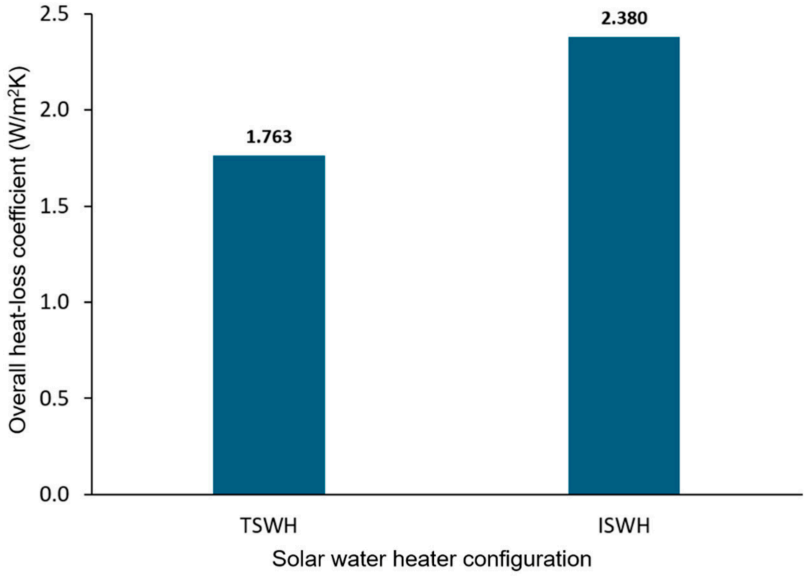

Figure 17. Overall heat-loss coefficient of the TSWH and ISWH prototypes.

Table 3. Comparison of the present study with previous experimental studies on passive solar water heaters.

Study	Climatic Conditions	Design Description	Findings
Kataria et al. [31]	New Delhi, India	- Concrete solar collector.	Water temperature between 42 and 50 °C.
Karaghouli and Alnasser [32]	Bahrain (Winter)	- Flat plate solar collector: TSWH. - Oriented to the south at a tilt angle of 36°.	Thermal efficiency = 38%. Hot water temperature = 50 °C.
Freegah and Al-Tabbakh [33]	Baghdad, Iraq (March days)	- Flat plate solar collector: TSWH. - Title angle of 53°.	Water temperature of approximately 34 °C.
Hazami et al. [34]	Jodhpur, India (from November 2007 to February 2008)	- Integrated Solar Storage Collector Based on Concrete Matrix. - Mass flow rate = 0.04 Kg/s.	Thermal efficiency = 32%. Hot water temperature = 50 °C.
Afeti et al. [35]	Nigeria (April and May)	- TSWH: The collector was oriented at a 30° tilt from the horizontal, with an azimuth angle of 15° east of south. - Absorber area of 1.4 m^2.	Thermal efficiency = 39%. Hot water temperature between 40 and 50 °C.
Present study	Gabes, Tunisia (March)	- Flat plate solar collector: TSWH and ISWH. Oriented to the south at a tilt angle of 90°.	Maximum water temperature of 59.8 °C for the ISWH and 53.65 °C for the TSWH; maximum thermal efficiency of 49% for the ISWH and 41% for the TSWH.

https://doi.org/10.3390/solar6040041

5. Conclusions

This study experimentally compared the thermal performance, heat-retention behaviour, and useful hot-water production of two vertically oriented passive solar water heating systems under arid outdoor conditions in Gabes, Tunisia. The investigated systems were a thermosiphon solar water heater (TSWH) and an integrated solar water heater (ISWH). Both prototypes were tested under the same climatic exposure, orientation, and collector area, allowing a direct comparison of their thermal behaviour under no-load and load conditions. The maximum measured solar flux was approximately 712 W/m^2 on 13 March 2023 and 708 W/m^2 on 14 March 2023. Under these conditions, the ISWH achieved higher maximum water temperatures than the TSWH. The ISWH reached 59.8 °C and 57.5 °C during the two test days, whereas the TSWH reached 48.55 °C and 53.65 °C. The ISWH also showed higher peak thermal efficiencies, reaching approximately 49% and 48%, compared with approximately 41% and 40% for the TSWH.

The results demonstrate a clear performance trade-off between the two configurations. The ISWH provided stronger daytime heat capture and higher useful hot-water production, delivering approximately 25 L of hot water at 45 °C under extraction conditions. In comparison, the TSWH delivered approximately 19 L. However, the TSWH showed better thermal retention during non-solar periods, as indicated by its lower overall heat-loss coefficient of approximately 1.763 W/m^{2}K compared with 2.38 W/m^{2}K for the ISWH.

These findings indicate that the ISWH is more suitable when rapid daytime heating and higher hot-water production are required, while the TSWH is more appropriate when improved heat preservation after solar input decreases is important. Therefore, the choice between the two configurations should depend on user demand patterns, building-integration requirements, and the expected timing of hot-water use.

Future work should focus on improving both the hot-water output and thermal retention of passive solar water heating systems. This could be achieved through absorber optimization, improved insulation, refined collector and storage design, and the incorporation of suitable thermal storage materials. Longer-term testing over different seasons would also be valuable for assessing annual performance under variable climatic conditions.

Author Contributions: W.Z., R.B.S., B.C., and A.B. conceived the study and developed the methodology. W.Z., R.B.S., B.C., and A.B. performed the formal analysis and contributed to data visualization. W.Z. and R.B.S. developed the software. W.Z., R.B.S., B.C., and A.B. prepared the original draft of the manuscript. S.A.K. contributed to the formal analysis and manuscript revision. A.A. contributed to the formal analysis, project administration, and manuscript revision. All authors have read and agreed to the published version of the manuscript.

Funding: The authors received no specific funding for this work.

Institutional Review Board Statement: This article does not contain any studies involving human participants or animals performed by any of the authors.

Data Availability Statement: Data is contained within the article.

Acknowledgments: The authors express their gratitude to the Tunisian Ministry of Higher Education and Scientific Research for the financing of this project given to their research group (LEEEP).

Conflicts of Interest: The authors declare no competing interests.

Nomenclature

Cp	Specific heat of water (J/Kg k)
G	Incident solar flux (W/m^2)
m	Mass of water (Kg)

T	Temperature (°C)
t	Time (second)
U	heat-loss coefficient (W/m^{2}K)
Abbreviations	
DST	Dynamic system testing
EN	European norm
FPSWH	Flat plate solar water heater
ISWH	Integrated solar water heater
TSWH	Thermosiphon solar water heater
SWH	Solar water heater
Greek symbols	
Δ	Variation
η	Efficiency
ρ	Density (Kg/m^3)
Subscripts	
Am	Ambient
f	final
i	Initial

References

1. Zaafouri, W.; Bouabidi, A.; Ben Slama, R.; Chaouachi, B.; Askar, A.H.; Kadhim, S.A. Experimental Study of a New Vertical Solar Water Heater Design under Varied Seasonal Weather Conditions in Gabes City. *Results Eng.* **2025**, *28*, 107197. [CrossRef]
2. Kadhim, S.A.; Ibrahim, O.A.A.-M.; Al-Ghezi, M.K.S.; Ashour, A.M.; Omle, I.; Bouabidi, A. Influence of the Steel Fibers Amount inside the Box on the Solar Cooker Performance: An Experimental Approach. *Results Eng.* **2025**, *26*, 105659. [CrossRef]
3. Zaafouri, W.; Ben Amara, W.; Bouabidi, A.; Kadhim, S.A.; Ashour, A.M.; Slama, R. Ben Thermal Performance Evaluation of a Closed-Loop Solar Water Heating System Under Variable Climatic Conditions. In *Proceedings of the 2025 IEEE International Multi-Conference on Smart Systems & Green Process (IMC-SSGP), Hammamet, Tunisia, 30 October 2025–2 November 2025*; IEEE: New York, NY, USA, 2025; pp. 1–6.
4. Sadhishkumar, S.; Balusamy, T. Performance Improvement in Solar Water Heating Systems—A Review. *Renew. Sustain. Energy Rev.* **2014**, *37*, 191–198. [CrossRef]
5. Al-Maliki, W.A.K.; Khafaji, H.Q.A.; Abdul Wahhab, H.A.; Al-Khafaji, H.M.H.; Alobaid, F.; Epple, B. Advances in Process Modelling and Simulation of Parabolic Trough Power Plants: A Review. *Energies* **2022**, *15*, 5512. [CrossRef]
6. Kumar, Y.; Verma, M.; Ghritlahre, H.K.; Verma, P. Recent Developments in the Thermal Performance of Flat Plate Solar Water Heaters with Reflectors-A Review. *Energy Sources Part A Recovery Util. Environ. Eff.* **2022**, *44*, 9448–9475. [CrossRef]
7. Alawee, W.H.; Hammoodi, K.A.; Dhahad, H.; Omara, Z.M.; Essa, F.; Abdullah, A.S.; Amro, M. Effects of Magnetic Field on the Performance of Solar Distillers: A Review Study. *Eng. Technol. J.* **2022**, *41*, 121–131. [CrossRef]
8. Shrivastava, R.L.; Vinod, K.; Untawale, S.P. Modeling and Simulation of Solar Water Heater: A TRNSYS Perspective. *Renew. Sustain. Energy Rev.* **2017**, *67*, 126–143. [CrossRef]
9. Dehghan, M.; Pfeiffer, C.F.; Rakhshani, E.; Bakhshi-Jafarabadi, R. A Review on Techno-Economic Assessment of Solar Water Heating Systems in the Middle East. *Energies* **2021**, *14*, 4944. [CrossRef]
10. Tian, Y.; Zhao, C.Y. A Review of Solar Collectors and Thermal Energy Storage in Solar Thermal Applications. *Appl. Energy* **2013**, *104*, 538–553. [CrossRef]
11. Gaonwe, T.P.; Kusakana, K.; Hohne, P.A. A Review of Solar and Air-Source Renewable Water Heating Systems, under the Energy Management Scheme. *Energy Rep.* **2022**, *8*, 1–10. [CrossRef]
12. Patel, K.; Patel, P.; Patel, J. Review of Solar Water Heating Systems. *Int. J. Adv. Eng. Technol.* **2012**, *3*, 146–149. [CrossRef]
13. Ben Slama, R. Experimentation of a Plane Solar Integrated Collector Storage Water Heater. *Energy Power Eng.* **2012**, *04*, 67–76. [CrossRef]
14. Zaafouri, W.; Ben Amara, W.; Bouabidi, A.; Kadhim, S.A.; Askar, A.H. Advancements and Integration Strategies of Solar Water Heaters in Buildings: A Comprehensive Review. *Energy Nexus* **2025**, *20*, 100535. [CrossRef]
15. Vera-Medina, J.; Fernandez-Peruchena, C.; Guasumba, J.; Lillo-Bravo, I. Performance Analysis of Factory-Made Thermosiphon Solar Water Heating Systems. *Renew. Energy* **2021**, *164*, 1215–1229. [CrossRef]
16. Kessentini, H.; Bouden, C. Numerical and Experimental Study of an Integrated Solar Collector with CPC Reflectors. *Renew. Energy* **2013**, *57*, 577–586. [CrossRef]

17. Kalogirou, S.A.; Papamarcou, C. Modelling of a Thermosyphon Solar Water Heating System and Simple Model Validation. *Renew. Energy* **2000**, *21*, 471–493. [CrossRef]
18. Sakellariou, E.I.; Axaopoulos, P.J.; Bot, B.V.; Kavadias, K.A. First Law Comparison of a Forced-Circulation Solar Water Heating System with an Identical Thermosyphon. *Energies* **2022**, *16*, 431. [CrossRef]
19. Messaouda, A.; Hamdi, M.; Hazami, M.; Guizani, A.A. Energetic and Economic Analysis of a New Integrated Collector Storage with Honeycomb Transparent Insulation (ICSHTI). *Environ. Prog. Sustain. Energy* **2020**, *39*, e13428. [CrossRef]
20. Hadjiat, M.M.; Hazmoune, M.; Ouali, S.; Gama, A.; Yaiche, M.R. Design and Analysis of a Novel ICS Solar Water Heater with CPC Reflectors. *J. Energy Storage* **2018**, *16*, 203–210. [CrossRef]
21. Souliotis, M.; Tripanagnostopoulos, Y. Experimental Study of CPC Type ICS Solar Systems. *Sol. Energy* **2004**, *76*, 389–408. [CrossRef]
22. Panaras, G.; Mathioulakis, E.; Belessiotis, V. A Method for the Dynamic Testing and Evaluation of the Performance of Combined Solar Thermal Heat Pump Hot Water Systems. *Appl. Energy* **2014**, *114*, 124–134. [CrossRef]
23. Kalogirou, S.A. Solar Thermal Collectors and Applications. *Prog. Energy Combust. Sci.* **2004**, *30*, 231–295. [CrossRef]
24. Harrabi, I.; Hamdi, M.; Hazami, M. Assessment of Uncertainties in Energetic and Exergetic Performances of a Flat Plate Solar Water Heater. *Math. Probl. Eng.* **2020**, *2020*, 6671576. [CrossRef]
25. Harrabi, I.; Hamdi, M.; Hazami, M. Potential of Simple and Hybrid Nanofluid Enhancement in Performances of a Flat Plate Solar Water Heater under a Typical North-African Climate (Tunisia). *Environ. Sci. Pollut. Res.* **2022**, *30*, 35366–35383. [CrossRef] [PubMed]
26. Liu, R.; Duan, W.; He, G.; Wang, Q. Development of Wall-Integrated Solar Energy Technologies. *Energies* **2025**, *18*, 952. [CrossRef]
27. Souliotis, M.; Singh, R.; Papaefthimiou, S.; Lazarus, I.J.; Andriosopoulos, K. Integrated Collector Storage Solar Water Heaters: Survey and Recent Developments. *Energy Syst.* **2016**, *7*, 49–72. [CrossRef]
28. Tripanagnostopoulos, Y.; Souliotis, M.; Nousia, T. CPC Type Integrated Collector Storage Systems. *Sol. Energy* **2002**, *72*, 327–350. [CrossRef]
29. Bouadila, S.; Baddadi, S.; Rehman, T.; Ayed, R. Experimental Investigation on the Thermal Appraisal of Heat Pipe-Evacuated Tube Collector-Based Water Heating System Integrated with PCM. *Renew. Energy* **2022**, *199*, 382–394. [CrossRef]
30. Shaltout, M.A.M.; Hassan, A.H.; Fathy, A.M. Total Suspended Particles and Solar Radiation over Cairo and Aswan. *Renew. Energy* **2001**, *23*, 605–619. [CrossRef]
31. Kataria, V.; Mahajan, S.; Singh, S.; Rana, V.; Mittal, P. Concrete Solar Collector. *Int. Res. J. Eng. Technol.* **2019**, *6*, 5053–5055.
32. Karaghouli, A.A.; Alnaser, W.E. Experimental Study on Thermosyphon Solar Water Heater in Bahrain. *Renew. Energy* **2001**, *24*, 389–396. [CrossRef]
33. Freegah, B.; Al-Tabbakh, A.A. Experimental and Numerical Analysis of a Thermosyphon Solar Water Heater for Domestic Applications. *UPB Sci. Bull. Ser. D Mech. Eng.* **2019**, *81*, 117–132.
34. Hazami, M.; Kooli, S.; Lazâar, M.; Farhat, A.; Belghith, A. Energetic and Exergetic Performances of an Economical and Available Integrated Solar Storage Collector Based on Concrete Matrix. *Energy Convers. Manag.* **2010**, *51*, 1210–1218. [CrossRef]
35. Afeti, G.M.; Imide, N.E.; Aiyedun, P.O. Experimental Investigation of a Partially Insulated Solar Water Heater with Natural Circulation. *Energy Convers. Manag.* **1991**, *32*, 145–151. [CrossRef]

https://doi.org/10.3390/solar6040041